Superdeformed and hyperdeformed states in $Z = 122$ isotopes

S. K. Patra,[1] M. Bhuyan,[1,2] M. S. Mehta,[3,4] and Raj K. Gupta[3]
[1]*Institute of Physics, Sachivalaya Marg, Bhubaneswar 751 005, India*
[2]*School of Physics, Sambalpur University, Jyotivihar, Burla 768 019, India*
[3]*Department of Physics, Panjab University, Chandigarh 160 014, India*
[4]*Department of Applied Sciences, RBCEBTW, Mohali 140 104, India*
(Received 29 April 2009; published 18 September 2009)

We calculate the binding energy, root-mean-square radius, and quadrupole deformation parameter for the recent, possibly discovered superheavy element $Z = 122$, using the axially deformed relativistic mean-field (RMF) and nonrelativistic Skyrme Hartree-Fock (SHF) formalisms. The calculation is extended to include various isotopes of $Z = 122$ element, starting from $A = 282$ to $A = 320$. We predict highly deformed structures in the ground state for all the isotopes. A shape transition appears at about $A = 290$ from a highly oblate to a large prolate shape, which may be considered as the superdeformed and hyperdeformed structures of the $Z = 122$ nucleus in the mean-field approaches. The most stable isotope (largest binding energy per nucleon) is found to be $^{302}122$, instead of the experimentally observed $^{292}122$.

DOI: 10.1103/PhysRevC.80.034312 PACS number(s): 21.10.Dr, 21.60.Jz, 23.60.+e, 27.90.+b

I. INTRODUCTION

The stability of nuclei in the superheavy mass region was predicted in the mid-sixties [1–4] when shell correction was added to the liquid drop binding energy and possible shell closure was pointed out at $Z = 114$ and $N = 184$. A nice historical review on theoretical predictions and new experimental possibilities is available in Ref. [5]. Myers and Swiatecki [6] concluded that the half-lives of nuclei near the shell closures must be long enough to be observed. In other words, nuclei with zero shell effects would not be stable and would decay immediately, as was predicted by macroscopic liquid drop models for $Z > 100$ nuclides. Recently, however, the microscopic studies of the nuclei beyond $Z = 100$ has become possible [7], and the heaviest nucleus studied so far in this series of experiments [8] is ^{254}No ($Z = 102$, $N = 152$). Thus, the progress in experimental techniques has drawn our attention and opened up the field once again for further theoretical investigations in structure physics of nuclei in the superheavy mass region.

Even though, experimentally, the elements up to $Z = 118$ have been synthesized to-date, with half-lives varying from a few minutes to milliseconds [9,10], the above-mentioned theoretically predicted center of the island of stability could not be located precisely. Recently, more microscopic theoretical calculations have predicted various other regions of stability, namely, $Z = 120$, $N = 172$ or 184 [11–13] and $Z = 124$ or 126, $N = 184$ [14,15]. Apparently, there is a need to design the new experiments to solve the outstanding problem of locating the precise island of stability for superheavy elements. In an effort in this direction, using inductively coupled plasma-sector field mass spectroscopy, Marinov *et al.* [16] have observed some neutron-deficient Th isotopes in naturally occurring Thorium substances. Long-lived isomeric states, with estimated half-lives $T_{1/2} \geqslant 10^8$ y, have been identified in the neutron-deficient ^{211,213,217,218}Th isotopes, which are associated with the superdeformed (SD) or hyperdeformed (HD) states (minima) in potential energy surfaces (PES). In a similar search for long-lived transactinides in natural materials, more recently, these authors [17] obtained a possible evidence for the existence of a long-lived superheavy nucleus with mass number $A = 292$ and atomic number $Z = 122$ or 124 in natural thorium. The half-life is again estimated to be the same as above, i.e., $T_{1/2} \geqslant 10^8$ y and abundance $(1–10) \times 10^{-12}$ relative to ^{232}Th. Note, however, that, although this discovery of an extremely superheavy nucleus is important, these results have yet to be confirmed by any other group. In any case, the very possibility of an extremely heavy Z nucleus motivated us to see the structures of such nuclei in an isotopic mass chain. Therefore, on the basis of the relativistic mean-field (RMF) and nonrelativistic Skyrme Hartree-Fock (SHF) methods, we calculated the bulk properties of a $Z = 122$ nucleus in an isotopic chain of mass $A = 282–320$. This choice of mass range covers both the predicted neutron magic numbers $N = 172$ and 184.

The article is organized as follows. Section II gives a brief description of the relativistic and nonrelativistic mean-field formalisms. The effects of pairing for open shell nuclei, included in our calculations, are also discussed in this section. The results of our calculations are presented in Sec. III, and a summary of the results obtained, together with concluding remarks, is given in Sec. IV.

II. THEORETICAL FRAMEWORK

A. The Skyrme Hartree-Fock method

The general form of the Skyrme effective interaction, used in the mean-field models, can be expressed as an energy density functional $\mathcal{H}$ [18,19],

$$\mathcal{H} = \mathcal{K} + \mathcal{H}_0 + \mathcal{H}_3 + \mathcal{H}_{\rm eff} + \cdots, \tag{1}$$

where $\mathcal{K} = \frac{\hbar^2}{2m}\tau$ is the kinetic energy term with m as the nucleon mass, $\mathcal{H}_0$ the zero range, $\mathcal{H}_3$ the density dependent term, and $\mathcal{H}_{\rm eff}$ the effective-mass dependent term, relevant for calculating the properties of nuclear matter, are functions of

nine parameters, t_i, x_i ($i = 0, 1, 2, 3$), and η, given as

$$\mathcal{H}_0 = \tfrac{1}{4}t_0\left[(2+x_0)\rho^2 - (2x_0+1)\left(\rho_p^2+\rho_n^2\right)\right], \quad (2)$$

$$\mathcal{H}_3 = \tfrac{1}{24}t_3\rho^\eta\left[(2+x_3)\rho^2 - (2x_3+1)\left(\rho_p^2+\rho_n^2\right)\right], \quad (3)$$

$$\mathcal{H}_{\text{eff}} = \tfrac{1}{8}\left[t_1(2+x_1)+t_2(2+x_2)\right]\tau\rho + \tfrac{1}{8}\left[t_2(2x_2+1)-t_1(2x_1+1)\right](\tau_p\rho_p+\tau_n\rho_n). \quad (4)$$

The other terms, representing the surface contributions of a finite nucleus with b_4 and b_4' as additional parameters, are

$$\mathcal{H}_{S\rho} = \tfrac{1}{16}\left[3t_1\left(1+\tfrac{1}{2}x_1\right)-t_2\left(1+\tfrac{1}{2}x_2\right)\right](\vec{\nabla}\rho)^2 - \tfrac{1}{16}\left[3t_1\left(x_1+\tfrac{1}{2}\right)+t_2\left(x_2+\tfrac{1}{2}\right)\right] \times[(\vec{\nabla}\rho_n)^2+(\vec{\nabla}\rho_p)^2], \quad (5)$$

and

$$\mathcal{H}_{S\vec{J}} = -\tfrac{1}{2}[b_4\rho\vec{\nabla}\cdot\vec{J}+b_4'(\rho_n\vec{\nabla}\cdot\vec{J}_n+\rho_p\vec{\nabla}\cdot\vec{J}_p)]. \quad (6)$$

Here, the total nucleon number density $\rho = \rho_n + \rho_p$, the kinetic energy density $\tau = \tau_n + \tau_p$, and the spin-orbit density $\vec{J} = \vec{J}_n + \vec{J}_p$, with n and p referring to neutron and proton, respectively. The $\vec{J}_q = 0, q = n$ or p, for spin-saturated nuclei, i.e., for nuclei with major oscillator shells completely filled. The total binding energy (BE) of a nucleus is the integral of the energy density functional $\mathcal{H}$. We have used here the Skyrme SkI4 set with $b_4 \neq b_4'$ [20], designed for considerations of proper spin-orbit interaction in finite nuclei, related to the isotope shifts in the Pb region.

B. The relativistic mean-field method

The relativistic Lagrangian density for a nucleon-meson many-body system [21,22] is written as

$$\mathcal{L} = \overline{\psi_i}\{i\gamma^\mu\partial_\mu - M\}\psi_i + \tfrac{1}{2}\partial^\mu\sigma\partial_\mu\sigma - \tfrac{1}{2}m_\sigma^2\sigma^2 - \tfrac{1}{3}g_2\sigma^3 - \tfrac{1}{4}g_3\sigma^4 - g_s\overline{\psi_i}\psi_i\sigma - \tfrac{1}{4}\Omega^{\mu\nu}\Omega_{\mu\nu} + \tfrac{1}{2}m_w^2V^\mu V_\mu + \tfrac{1}{4}c_3(V_\mu V^\mu)^2 - g_w\overline{\psi}_i\gamma^\mu\psi_i V_\mu - \tfrac{1}{4}\vec{B}^{\mu\nu}.\vec{B}_{\mu\nu} + \tfrac{1}{2}m_\rho^2\vec{R}^\mu.\vec{R}_\mu - g_\rho\overline{\psi}_i\gamma^\mu\vec{\tau}\psi_i.\vec{R}^\mu - \tfrac{1}{4}F^{\mu\nu}F_{\mu\nu} - e\overline{\psi}_i\gamma^\mu\tfrac{(1-\tau_{3i})}{2}\psi_i A_\mu. \quad (7)$$

All the quantities have their usual well-known meanings. From the above Lagrangian we obtain the field equations for the nucleons and mesons. These equations are solved by expanding the upper and lower components of the Dirac spinors and the boson fields in an axially deformed harmonic oscillator basis with an initial deformation β_0. The set of coupled equations is solved numerically by a self-consistent iteration method. The center-of-mass motion energy correction is estimated by the usual harmonic oscillator formula $E_{\text{c.m.}} = \frac{3}{4}(41A^{-1/3})$. The quadrupole deformation parameter β_2 is evaluated from the resulting proton and neutron quadrupole moments as $Q = Q_n + Q_p = \sqrt{\frac{16\pi}{5}}(\frac{3}{4\pi}AR^2\beta_2)$. The root-mean-square (rms) matter radius is defined as $\langle r_m^2\rangle = \frac{1}{A}\int\rho(r_\perp, z)r^2d\tau$, where A is the mass number and $\rho(r_\perp, z)$ is the deformed density. The total binding energy and other observables are also obtained by using the standard relations, given in Ref. [22]. We use the well-known NL3 parameter set [23]. This set not only reproduces the properties of stable nuclei but also well predicts for those far from the β-stability valley. As outputs, we obtain different potentials, densities, single-particle energy levels, radii, deformations, and binding energies. For a given nucleus, the maximum binding energy corresponds to the ground state and other solutions are obtained as various excited intrinsic states.

C. Pairing effect

Pairing is a crucial quantity for open shell nuclei in determining the nuclear properties. The constant gap, BCS-pairing approach is reasonably valid for nuclei in the valley of the β-stability line. However, this method breaks down when the coupling of the continuum becomes important. In the present study, we deal with nuclei on or near the valley of the stability line because the superheavy elements, though very exotic in nature, lie on the β-stability line. These nuclei are unstable because of the repulsive Coulomb force, but the attractive nuclear shell effects come to their rescue, making the superheavy element possible to be synthesized, particularly when a combination of magic proton and neutron number happens to occur (largest shell correction).

The pairing energy expression $E_{\text{pair}} = -G[\sum_{i>0}u_iv_i]^2$, where G is the pairing force constant and v_i^2 and $u_i^2 = 1 - v_i^2$ are the occupation probabilities [22,24,25]. The variational procedure with respect to the occupation numbers v_i^2 gives the BCS equation $2\epsilon_iu_iv_i - \triangle(u_i^2 - v_i^2) = 0$, with $\triangle = G\sum_{i>0}u_iv_i$. This is the famous BCS equation for pairing energy. The densities are contained within the occupation number $n_i = v_i^2 = \frac{1}{2}[1 - \frac{\epsilon_i-\lambda}{\sqrt{(\epsilon_i-\lambda)^2+\triangle^2}}]$. To take care of the pairing effects in the present study, we use the constant gap for proton and neutron, as given in Ref. [26]: $\triangle_p = RB_se^{sI-tI^2}/Z^{1/3}$ and $\triangle_n = RB_se^{-sI-tI^2}/A^{1/3}$, with $R = 5.72$, $s = 0.118$, $t = 8.12$, $B_s = 1$, and $I = (N-Z)/(N+Z)$. (Note that the gaps obtained by these expressions are valid for nuclei both on or away from the stability line.) The pairing force constant G is not calculated explicitly in solving the RMF equations. Using the above gap parameter, we calculate directly the occupation probability. The chemical potentials λ_n and λ_p are determined by the particle numbers for protons and neutrons. Finally, we can write the pairing energy as $E_{\text{pair}} = -\triangle\sum_{i>0}u_iv_i$. Apparently, in a given nucleus, for a constant pairing gap $\triangle$, the pairing energy E_{pair} is not constant because it depends on the occupation probabilities v_i^2 and u_i^2, and hence on the deformation parameter β_2, particularly near the Fermi surface. It is known that for a constant pairing parameter $\triangle$ and force constant G, the pairing energy E_{pair} diverges if it is extended to an infinite configuration space. In fact, in all realistic calculations with finite range forces, $\triangle$ decreases with state (spherical or deformed) for large momenta near the Fermi surface. However in the present case, we assume that pairing gap for all states $|\alpha\rangle = |nljm\rangle$ are equal to each other near the Fermi surface and hence a constant pairing gap is taken for simplicity of the calculations. We use in our calculations, a pairing window, and all the equations are extended up to the level $\epsilon_i - \lambda \leqslant 2(41A^{1/3})$. The factor 2 has been determined so as to reproduce the pairing correlation energy for neutrons in ^{118}Sn using Gogny force [22,24]. This type of prescription for

pairing effects, in both RMF and SHF models, has already been used by us and by many other authors [22,24,27]. Within this pairing approach, it is shown [27,28] that the results for binding energies and quadruple deformations are almost identical with the predictions of the relativistic Hartree-Bogoliubov (RHB) approach [28,29].

III. RESULTS AND DISCUSSION

A. Ground state properties using the SHF and RMF models

There exist a number of parameter sets for solving the standard SHF Hamiltonians and RMF Lagrangians. In many of our previous works and those of other authors [13,22,23, 30–32] the ground state properties, like the binding energies (BE), quadrupole deformation parameters β_2, charge radii (r_c), and other bulk properties, are evaluated by using the various nonrelativistic and relativistic parameter sets. It is found that, more or less, most of the recent parameter sets reproduce well the ground state properties, not only of stable normal nuclei but also of exotic nuclei that are far away from the valley of β stability. This means that if one uses a reasonably acceptable parameter set, the predictions of the model will remain nearly force independent.

B. Potential energy surface

In this subsection, we first calculate the potential energy surfaces (PES) by using both the RMF and SHF theories in a constrained calculation [32–36], i.e., instead of minimizing the H_0, we have minimized $H' = H_0 - \lambda Q_2$, with λ as a Lagrange multiplier and Q_2, the quadrupole moment. Thus, we get the solution at a given quadrupole deformation. Here, H_0 is a Dirac mean-field Hamiltonian (the notations are standard and its form can be seen in Refs. [22,34,36]) in the RMF model and it is a Schrödinger mean-field Hamiltonian in the SHF model. In other words, we get the constrained solution from the minimization $\sum_{ij} \frac{\langle\psi_i|H_0-\lambda Q_2|\psi_j\rangle}{\langle\psi_i|\psi_j\rangle}$ and then calculate the constrained energy using H_0. The "free energy" is obtained from BE $= \sum_{ij} \frac{\langle\psi_i|H_0|\psi_j\rangle}{\langle\psi_i|\psi_j\rangle}$. In our calculations, the free energy solution does not depend on the initial guess value of the basis deformation β_0 as long as it is nearer to the minimum in PES. However it converges to some other local minimum when β_0 is drastically different, and in this way we evaluate a different isomeric state for a given nucleus.

The PES, i.e., the potential energy as a function of quadrupole deformation parameter β_2, for the superheavy nucleus $^{292}122$, is shown in Fig. 1. Both the RMF and SHF results are given for comparisons. The calculated PES is shown for a wide range of oblate to prolate deformations. We notice from this figure that in RMF model, minima appear at around $\beta_2 = -0.436, -0.032$, and 0.523. The energy differences between the ground and the isomeric states are found to be 0.48 and 1.84 MeV for the nearest consecutive minimas. For the SHF model, the minima appear at around $\beta_2 = -0.459, -0.159$, and 0.511. The intrinsic excited state energy differences are 1.30 and 0.48 MeV. From the figure it is clear that the minima and the maxima in both the RMF and SHF

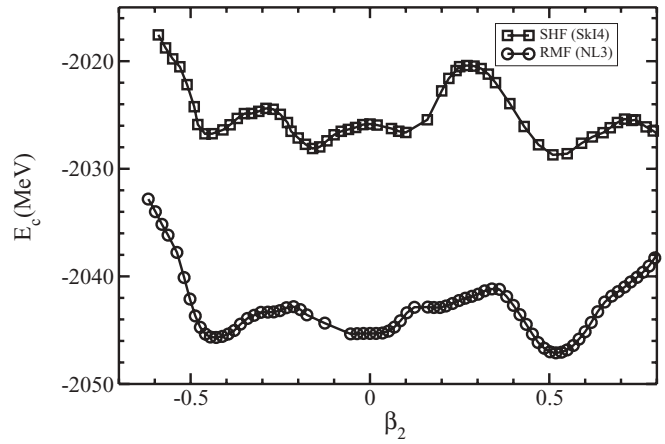

FIG. 1. The potential energy surfaces for the $^{292}122$ nucleus as a function of the quadrupole deformation parameter. The open squares with the solid line represent SHF calculations using the SkI4 parameter set, and the open circles with the solid line represent RMF calculations using the NL3 parameter set.

models are qualitatively similar. The absolute values differ by a constant factor from one another, i.e., the two calculations (RMF and SHF) differ from each other by a large shift of $\sim$15 MeV. This difference, however, may be considered small for a nucleus because the binding energies per nucleon just differ from one another by a small factor of 0.075, as is shown in Fig. 4. In other words, this difference in PES is also reflected in the binding energy calculations of this nucleus in an isotopic chain, which is discussed in the following subsection.

C. Binding energy, two-neutron separation energy, and pairing energy

Figure 2 shows the calculated binding energy, obtained in both the SHF and RMF formalisms. We notice that, similar to the PES, the binding energy obtained in the RMF model also over-estimates the SHF result by a constant factor. In other words, here also the multiplication by a constant factor will

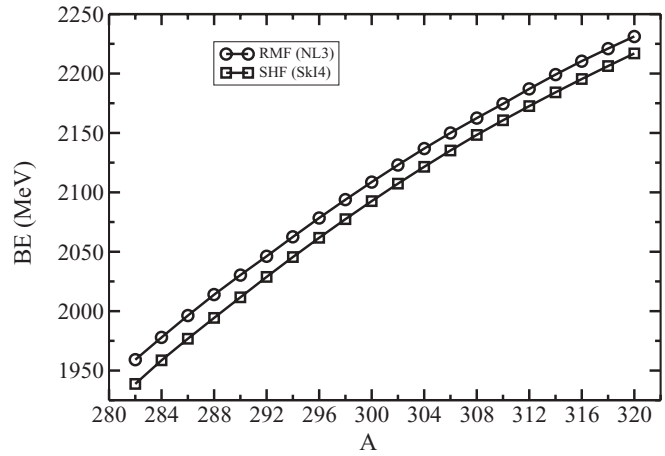

FIG. 2. The total binding energy for $^{282-320}122$ nuclei in SHF(SkI4) and RMF(NL3) calculations.

TABLE I. The SHF(SkI4) and the RMF(NL3) results for binding energy BE, two-neutron separation energy S_{2n}, and the quadrupole deformation parameter β_2, compared with the finite range droplet model (FRDM) data [37]. The energy is in MeV.

Nucleus	SHF(SkI4 parameter set)			RMF(NL3 parameter set)			FRDM results		
	BE	S_{2n}	β_2	BE	S_{2n}	β_2	BE	S_{2n}	β_2
294	2045.52	16.29	0.534	2062.49	16.71	0.530	2053.16		−0.155
296	2061.74	15.94	0.529	2078.46	16.21	0.527	2068.99	15.84	−0.130
298	2077.44	15.34	0.526	2093.81	15.70	0.536	2084.26	15.26	−0.096
300	2092.62	14.81	0.526	2108.67	15.18	0.548	2099.64	15.38	0.009
302	2107.30	14.34	0.529	2123.01	14.68	0.562	2113.98	14.34	0.418
304	2121.47	13.82	0.545	2136.83	14.17	0.603	2126.87	12.89	0.000
306	2132.71	13.20	0.556	2150.03	13.76	0.608	2139.43	12.56	0.000
308	2148.31	12.45	0.560	2162.49	13.08	0.618	2150.84	11.41	0.001
310	2160.66	12.00	0.571	2174.49	12.35	0.641	2162.05	11.22	0.003
312	2172.58	12.62	0.584	2187.10	11.92	0.742	2173.42	11.36	0.005
314	2184.17	12.02	0.594	2199.12	11.59	0.739	2184.67	11.25	0.006
316	2295.39	11.37	0.595	2210.49	11.22	0.736	2195.74	11.07	0.007
318	2206.30	10.65	0.588	2221.02	10.91	0.722	2214.11	18.37	0.541
320	2216.96	10.21	0.575	2231.23	10.67	0.728	2224.88	10.76	0.543

make the two curves overlap with one another. This means that a slight modification of the parameter set of one formalism can predict a binding energy similar to that of the other.

Table I shows a comparison of the calculated binding energies with the finite range droplet model (FRDM) predictions of Ref. [37], wherever possible. The two-neutron separation energy $S_{2n}(N,Z) = \mathrm{BE}(N,Z) - \mathrm{BE}(N-2,Z)$ is also listed in Table I. From the table, we find that the microscopic binding energies and the S_{2n} values agree well with the macro-microscopic FRDM calculations. The comparisons of S_{2n} for the SHF and RMF models with the FRDM result are further shown in Fig. 3, which shows clearly that the two S_{2n} values coincide remarkably well, except at mass $A = 318$ which seems spurious due to some error somewhere in the case of FRDM. Apparently, the S_{2n} valeus decrease gradually with increase of the neutron number, except for the noticeable kinks at $A = 294$ ($N = 172$) and 312 ($N = 190$) in RMF and at $A = 304$ ($N = 182$) and 308 ($N = 186$) in FRDM. Interestingly, these neutron numbers are close to either $N = 172$ or 184 magic numbers. However, the SHF results are smooth.

The binding energy per particle for the isotopic chain is also plotted in Fig. 4. We notice that here again the SHF and RMF curves could be overlapped with one another through a constant scaling factor, and the FRDM calculation lies in between these two calculations. This means, qualitatively, all three curves show a similar behavior. However, unlike the BE/A curve for SHF or RMF, the FRDM results do not show the regular behavior. In general, the BE/A value starts increasing with the increase of mass number A, reaching a peak value at $A = 302$ for all three formalisms. This means that $^{302}122$ is the most stable element from the binding energy

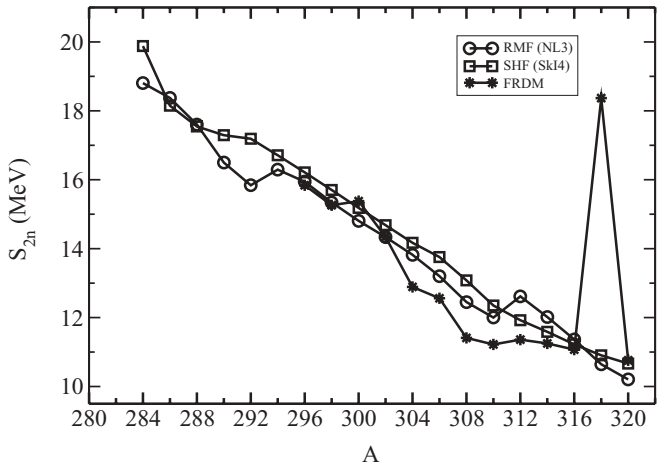

FIG. 3. The two-neutron separation energy S_{2n} for $^{282-320}122$ nuclei, obtained from SHF(SkI4) and RMF(NL3) formalisms and compared with the FRDM results [37] wherever available.

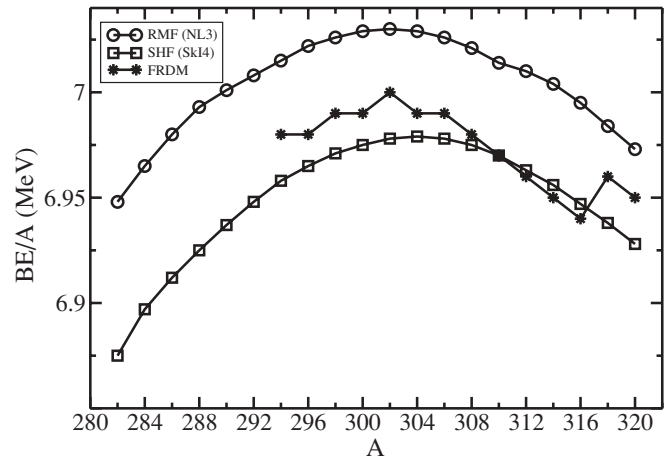

FIG. 4. The binding energy per particle BE/A for the superheavy isotopes $^{282-320}122$ obtained in SHF(SkI4) and RMF(NL3) formalisms compared with the FRDM results [37] wherever available.

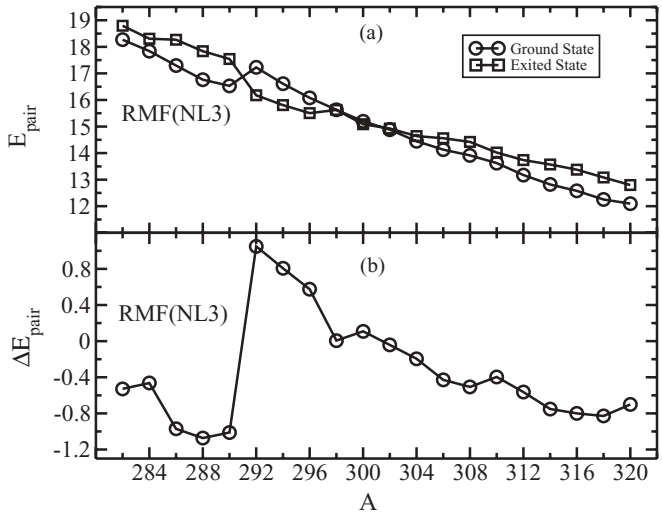

FIG. 5. (a) The pairing energy E_{pair} for the ground and first excited states and (b) the pairing energy difference ΔE_{pair} between the E_{pair} values of ground and first excited states [$\Delta E_{\text{pair}} = E_{\text{pair}}(\text{g.s.}) - E_{\text{pair}}(\text{e.s.})$] as a function of the mass of nucleus, using the relativistic mean-field formalism RMF(NL3).

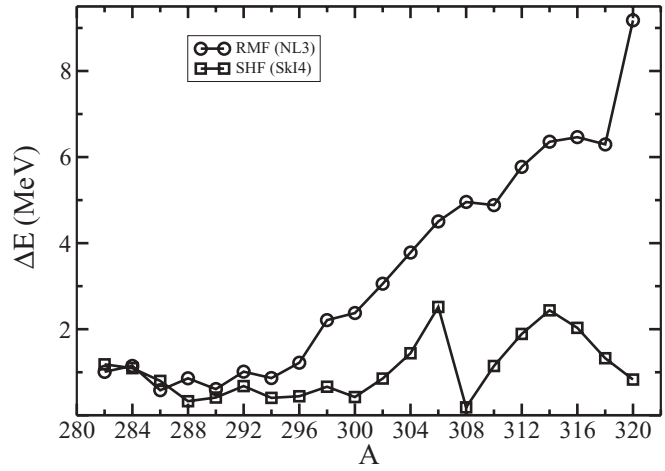

FIG. 6. The energy difference between the ground state and the first excited state in both nonrelativistic SHF(SkI4) and relativistic RMF(NL3) formalisms.

point of view. Interestingly, $^{302}122$ is situated toward the neutron-deficient side of the isotopic series of $Z = 122$ and could be taken as a suggestion to synthesize this superheavy nucleus experimentally.

Certainly, pairing is important for open shell nuclei. However, for a given nucleus, its value depends only marginally on the quadrupole deformation β_2. This means that for differing β_2 values in a nucleus, the pairing energy E_{pair} changes only marginally (∼5–6%). On the other hand, even if the β_2 values for two nuclei are same, the E_{pair} values are different from one another, depending on the filling of the nucleons. This result is illustrated in Fig. 5 for the RMF(NL3) calculation, where the pairing energy E_{pair} for both the ground state (g.s.) and the first excited state (e.s.), referring to different β_2 values, are plotted in panel (a) for the full isotopic chain. The difference in the two E_{pair} values, i.e., $\Delta E_{\text{pair}} = E_{\text{pair}}(\text{g.s.}) - E_{\text{pair}}(\text{e.s.})$, is given in Fig. 5(b). It is clear from Fig. 5(a) that E_{pair} decreases with an increase in mass number A; i.e., even if the β_2 values for two nuclei are the same, the pairing energies are different from one another. This change of the E_{pair} value is ∼25% in going from, say, $A = 294$ to 320. In Fig. 5(b), the ΔE_{pair} value is ∼5–6% of the E_{pair} for many of the nuclei because of their two different configurations (g.s. and first e.s.).

D. Shape coexistence

We have also calculated the "free solutions" for the whole isotopic chain, both in prolate and oblate deformed configurations. In many cases, we find low-lying excited states. As a measure of the energy difference between the ground band and the first excited state, we have plotted in Fig. 6 the binding energy difference $\triangle E$ between the two solutions, noting that the maximum binding energy solution refers to the ground state and all other solutions refer to the intrinsic excited state(s). From Fig. 6, we notice that, in RMF calculations, the energy difference $\triangle E$ is small for neutron-deficient isotopes, but it increases with the increase of mass number A in the isotopic series. This small difference in the binding energy for neutron-deficient isotopes is an indication of shape coexistence. In other words, the two solutions in these nuclei are almost degenerate and might have large shape fluctuations. On the other hand, in SHF formalism, the $\triangle E$ value remains small throughout the isotopic chain. For example, in $^{308}122$ the two solutions for $\beta_2 = 0.56$ and $\beta_2 = 0.008$ are completely degenerate with binding energies of 2148.31 and 2148.12 MeV. This later result suggests that the ground state can be changed to the excited state and vice versa by a small change in the input, like the pairing strength, etc., in the calculations. In any case, such a phenomenon is known to exist in many other regions [38] of the periodic table.

E. Quadrupole deformation parameter

The quadrupole deformation parameter β_2, for both the ground state and the first excited states, is also determined within the two formalisms. In some of the earlier RMF and SHF calculations, it was shown that the quadrupole moment obtained from these theories reproduce the experimental data pretty well [13,18,20–23,30,39,40]. We have seen in Fig. 1 that both the ground state and intrinsic excited quadrupole deformation parameters for SHF and RMF results agree well with each other (the same is true for "free solutions," not shown here). However, the ground state (g.s.) quadrupole deformation parameter β_2 values plotted in Fig. 7 for SHF and RMF formalisms, and compared with FRDM results [37], show that the FRDM results differ strongly. In both the SHF and RMF results, we find highly deformed oblates solutions in the g.s. configuration for isotopes near the low mass region. Then, with increase of mass number there is a shape change from highly oblate to highly prolate in both SHF and RMF models. Interestingly, most of the isotopes are superdeformed in their g.s. configurations, and because of the shape coexistence

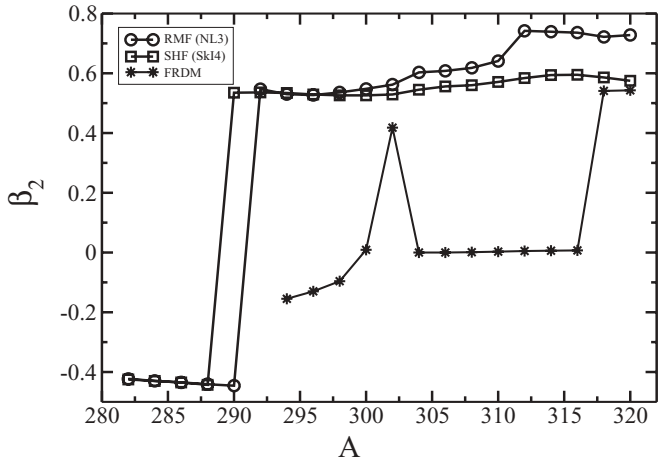

FIG. 7. Comparison of quadrupole deformation parameters obtained from nonrelativistic SHF formalism, SHF(SkI4), and relativistic mean-field formalism, RMF(NL3), compared with the FRDM results [37] wherever available.

properties of these isotopes, sometimes it is possible that the g.s. could be the hyperdeformed solution.

F. Nuclear radii

The rms radii for proton (r_p), neutron (r_n), and matter (r_m) distributions are shown in Figs. 8(a) and 8(b), respectively, for SHF and RMF formalisms. Figure 8(a) shows the SHF calculations and Fig. 8(b) the RMF calculations. As expected, the neutron and matter distribution radii increase with increases of the neutron number. Although, the proton number $Z = 122$ is constant in the isotopic series, the value of r_p also increases as shown in the figure. This trend is similar in both the formalisms. A detailed inspection of the figure shows that, in the RMF calculation, the radii show a jump at $A = 312$ ($N = 190$) after the monotonic increase of radii to $A = 310$. Note that a similar trend was observed in RMF calculations for S_{2n} (see Fig. 3).

G. The Q_α energy and the decay half-life T_α

We choose the nucleus $^{292}122$ ($Z = 122$, $N = 170$) for illustrating our calculations of the α-decay chain and the half-life time T_α. The Q_α energy is obtained from the relation [41]

$$Q_\alpha(N,Z) = \mathrm{BE}(N,Z) - \mathrm{BE}(N-2, Z-2) - \mathrm{BE}(2,2).$$

Here, BE(N,Z) is the binding energy of the parent nucleus with neutron number N and proton number Z, BE(2,2) is the binding energy of the α particle (^{4}He), i.e., 28.296 MeV, and BE$(N-2, Z-2)$ is the binding energy of the daughter nucleus after the emission of an α particle.

The binding energies of the parent and daughter nuclei are obtained by using both the RMF and SHF formalisms. Our predicted results are compared in Table II with the FRDM calculation of Ref. [37] and the experimental data [42,43], wherever possible. The Q_α values are then calculated; they are shown in Table II and in Fig. 9(b). Then, the half-life $\log_{10} T_\alpha(s)$ values are estimated by using the phenomenological formula of Viola and Seaborg [44]: $\log_{10} T_\alpha(s) = \frac{aZ-b}{\sqrt{Q_\alpha}} - (cZ + d)$, where Z is the atomic number of the parent nucleus, $a = 1.66175$, $b = 8.5166$, $c = 0.20228$, and $d = 33.9069$. The calculated $\log_{10} T_\alpha(s)$ values are also given in Table II and in Fig. 9(a).

From Figs. 9(a) and 9(b) and Table II, we notice that the calculated values for both Q_α and $T_\alpha(s)$ agree quite well with the FRDM predictions, as well as with the known experimental data. For example, the value of T_α, in both the FRDM and RMF model, coincides well with the data for the ^{264}Hs nucleus. Similarly, for $^{276}114$, the SHF prediction matches the FRDM result. Possible shell structure effects in Q_α, as well as in $T_\alpha(s)$, are noticed for the daughter nucleus $A = 256$ ($Z = 104$, $N = 152$) and 284 ($Z = 118$, $N = 166$) in SHF and for

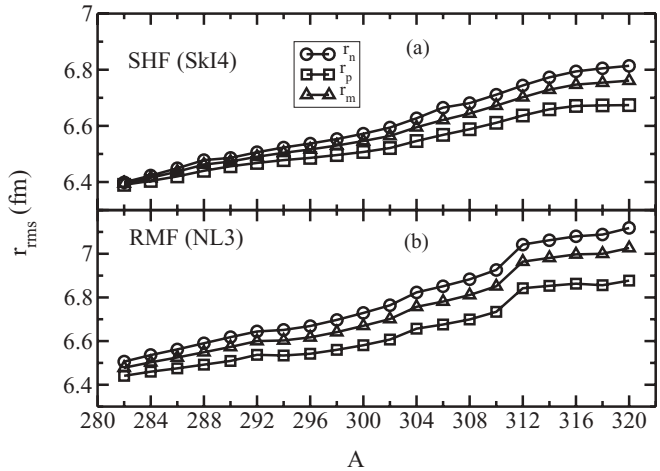

FIG. 8. The rms radii of proton (r_p), neutron (r_n), and matter (r_m) distributions for $^{282-320}122$ nuclei using (a) nonrelativistic SHF formalism, SHF(SkI4), and (b) relativistic mean-field formalism, RMF(NL3).

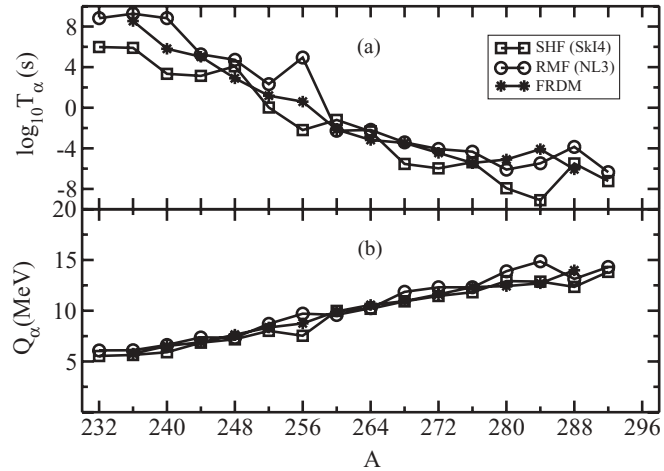

FIG. 9. (a) The half-life time T_α for $^{292}122$ nucleus and (b) the Q_α energy for the $^{292}122$ nucleus using the nonrelativistic SHF formalism, SHF(SkI4), the relativistic mean-field formalism, RMF(NL3), and the FRDM data [37].

TABLE II. The Q_α and T_α calculated in the SHF(SkI4) and the RMF(NL3) models and compared with the finite range droplet model (FRDM) results [37] as well as the experimental data [42,43], wherever available. The binding energies marked with an asterisk (*) are the extrapolated values. The energy is in MeV and the half-life time in seconds.

Nucleus	Z	SHF(SkI4 parameter set)			RMF(NL3 parameter set)			FRDM results			Experimental results		
		BE	Q_α	T_α	BE	Q_α	T_α	BE	Q_α	T_α	BE	Q_α	T_α
292	122	2028.81	14.31	$10^{-7.23}$	2046.19	13.83	$10^{-6.35}$						
288	120	2014.82	13.13	$10^{-5.49}$	2031.75	12.35	$10^{-3.85}$	2023.06	13.98	$10^{-6.07}$			
284	118	1999.65	14.86	$10^{-9.11}$	2015.80	12.87	$10^{-5.48}$	2008.69	12.70	$10^{-4.08}$			
280	116	1986.21	13.89	$10^{-7.93}$	2000.37	12.92	$10^{-6.10}$	1993.49	12.42	$10^{-5.10}$			
276	114	1971.80	12.30	$10^{-5.37}$	1984.99	11.82	$10^{-4.33}$	1977.62	12.33	$10^{-5.44}$			
272	112	1955.80	12.33	$10^{-5.97}$	1968.51	11.45	$10^{-4.07}$	1961.66	11.61	$10^{-4.45}$			
268	110	1939.83	11.86	$10^{-5.54}$	1951.66	10.92	$10^{-3.41}$	1944.97	10.94	$10^{-3.47}$	1943.00*	11.5	$10^{-4.76}$
264	108	1923.39	10.25	$10^{-2.34}$	1934.28	10.19	$10^{-2.19}$	1927.62	10.57	$10^{-3.18}$	1926.67	10.65	$10^{-3.3}$
260	106	1905.34	9.59	$10^{-1.10}$	1916.17	9.98	$10^{-2.27}$	1909.90	9.93	$10^{-2.15}$	1908.92	9.70	$10^{-1.5}$
256	104	1886.63	9.71	$10^{-2.20}$	1897.85	7.53	$10^{4.95}$	1891.53	8.75	$10^{0.59}$	1890.56	8.90	$10^{0.13}$
252	102	1868.04	8.71	$10^{0.02}$	1877.08	8.02	$10^{2.32}$	1871.98	8.35	$10^{1.19}$	1871.35*	8.50	$10^{0.67}$
248	100	1848.45	7.34	$10^{4.08}$	1856.80	7.18	$10^{4.72}$	1852.03	7.64	$10^{2.91}$	1851.57	8.0	$10^{1.60}$
244	98	1827.49	7.37	$10^{3.14}$	1835.68	6.85	$10^{5.26}$	1831.38	6.90	$10^{5.01}$	1831.22	7.32	$10^{3.30}$
240	96	1806.56	6.63	$10^{3.34}$	1814.23	5.91	$10^{8.82}$	1809.98	6.52	$10^{5.81}$	1805.52	6.40	$10^{6.36}$
236	94	1784.89	6.10	$10^{5.90}$	1791.84	5.64	$10^{9.26}$	1788.21	5.77	$10^{8.54}$	1788.41	5.87	$10^{8.03}$
232	92	1762.69	6.09	$10^{5.98}$	1768.19	5.54	$10^{8.82}$	1754.15	5.14	$10^{11.18}$	1765.98	5.41	$10^{9.50}$

$A = 256$ ($A = 104$, $N = 152$) and 288 ($Z = 120$, $N = 168$) in RMF calculations. Note that some of these proton or neutron numbers refer to either observed or predicted magic numbers.

IV. SUMMARY

Concluding, we have calculated the binding energy, rms radius, and quadrupole deformation parameter for the possibly discovered $Z = 122$ superheavy element recently. From the calculated binding energy, we also estimated the two-neutron separation energy for the isotopic chain. We employed both the SHF and RMF formalisms to see the formalism dependence of the results. We found qualitatively similar predictions in both techniques. A shape change from oblate to prolate deformation is observed with an increase of isotopic mass number at $A = 290$. The ground state structures are highly deformed, which are comparable to superdeformed or hyperdeformed solutions, in agreement with the observations of Ref. [17] for the superheavy region. From the binding energy analysis, we found that the most stable isotope in the series is $^{302}122$, instead of the observed $^{292}122$, considered to be a neutron-deficient nucleus. Our predicted α-decay energy Q_α and half-life time T_α agree nicely with the FRDM calculations and available experimental data. Some shell structure is also observed in the calculated quantities at $N = 172$ or 190 for RMF and at $N = 182$–186 for SHF calculations for the various isotopes of the $Z = 122$ nucleus.

ACKNOWLEDGMENTS

This work is supported in part by the Council of Scientific & Industrial Research (Project 03(1060)06/EMR-II) and by the Department of Science and Technology (DST), Government of India (Project SR/S2/HEP-16/2005).

[1] W. D. Myers and W. J. Swiatecki, Report UCRL 11980, 1965.
[2] A. Sobiczewski, F. A. Gareev, and B. N. Kalinkin, Phys. Lett. **22**, 500 (1966).
[3] H. Meldner, in Proceedings of the International Lysekil Symposium, Sweden, 21–27 August 1966; Ark. Fys. **36**, 593 (1967).
[4] U. Mosel and W. Greiner, Z. Phys. **222**, 261 (1969).
[5] B. N. Kalinkin and F. A. Gareev, arXiv:nucl-ex/0105021.
[6] W. D. Myers and W. J. Swiatecki, Nucl. Phys. **81**, 1 (1966).
[7] R. D. Herzberg, J. Phys. G: Nucl. Part. Phys. **30**, 123(R) (2004); M. Leino and F. P. Hessberger, Annu. Rev. Nucl. Part. Sci. **54**, 175 (2004).
[8] R. D. Herzberg *et al.*, Nature (London) **442**, 896 (2006).
[9] S. Hofmann and G. Münzenberg, Rev. Mod. Phys. **72**, 733 (2000).
[10] Yu. Oganessian, J. Phys. G: Nucl. Part. Phys. **34**, R165 (2007).
[11] K. Rutz, M. Bender, T. Bürvenich, T. Schilling, P.-G. Reinhard, J. A. Maruhn, and W. Greiner, Phys. Rev. C **56**, 238 (1997).
[12] R. K. Gupta, S. K. Patra, and W. Greiner, Mod. Phys. Lett. A **12**, 1727 (1997).
[13] S. K. Patra, C.-L. Wu, C. R. Praharaj, and R. K. Gupta, Nucl. Phys. **A651**, 117 (1999).
[14] S. Cwiok, J. Dobaczewski, P.-H. Heenen, P. Magierski, and W. Nazarewicz, Nucl. Phys. **A611**, 211 (1996); S. Cwiok, W. Nazarewicz, and P. H. Heenen, Phys. Rev. Lett. **83**, 1108 (1999).
[15] A. T. Kruppa, M. Bender, W. Nazarewicz, P.-G. Reinhard, T. Vertse, and S. Cwiok, Phys. Rev. C **61**, 034313 (2000).
[16] A. Marinov, I. Rodushkin, Y. Kashiv, L. Halicz, I. Segal, A. Pape, R. V. Gentry, H. W. Miller, D. Kolb, and R. Brandt, Phys. Rev. C **76**, 021303(R) (2007).

[17] A. Marinov, I. Rodushkin, D. Kolb, A. Pape, Y. Kashiv, R. Brandt, R. V. Gentry, and H. W. Miller, arXiv:0804.3869v1 [nucl-ex]; A. Marinov, I. Rodushkin, A. Pape, Y. Kashiv, D. Kolb, R. Brandt, R. V. Gentry, H. W. Miller, L. Halicz, and I. Segal, Int. J. Mod. Phys. E **18**, 621 (2009).
[18] E. Chabanat, P. Bonche, P. Hansel, J. Meyer, and R. Schaeffer, Nucl. Phys. **A627**, 710 (1997).
[19] J. R. Stone and P.-G. Reinhard, Prog. Part. Nucl. Phys. **58**, 587 (2007).
[20] P.-G. Reinhard and H. Flocard, Nucl. Phys. **A584**, 467 (1995).
[21] B. D. Serot and J. D. Walecka, Adv. Nucl. Phys. **16**, 1 (1986).
[22] Y. K. Gambhir, P. Ring, and A. Thimet, Ann. Phys. (NY) **198**, 132 (1990).
[23] G. A. Lalazissis, J. König, and P. Ring, Phys. Rev. C **55**, 540 (1997).
[24] S. K. Patra, Phys. Rev. C **48**, 1449 (1993).
[25] M. A. Preston and R. K. Bhaduri, *Structure of Nucleus* (Addison-Wesley, Reading, MA, 1982), Chap. 8, p. 309.
[26] D. G. Madland and J. R. Nix, Nucl. Phys. **A476**, 1 (1981); P. Möller and J. R. Nix, At. Data Nucl. Data Tables **39**, 213 (1988).
[27] S. K. Patra, M. Del Estal, M. Centelles, and X. Viñas, Phys. Rev. C **63**, 024311 (2001); T. R. Werner, J. A. Sheikh, W. Nazarewicz, M. R. Strayer, A. S. Umar, and M. Mish, Phys. Lett. **B335**, 259 (1994); T. R. Werner, J. A. Sheikh, M. Mish, W. Nazarewicz, J. Rikovska, K. Heeger, A. S. Umar, and M. R. Strayer, Nucl. Phys. **A597**, 327 (1996).
[28] G. A. Lalazissis, D. Vretenar, P. Ring, M. Stoitsov, and L. M. Robledo, Phys. Rev. C **60**, 014310 (1999).
[29] G. A. Lalazissis, D. Vretenar, and P. Ring, Nucl. Phys. **A650**, 133 (1999).
[30] P. Arumugam, B. K. Sharma, S. K. Patra, and R. K. Gupta, Phys. Rev. C **71**, 064308 (2005).
[31] S. K. Patra, R. K. Gupta, B. K. Sharma, P. D. Stevenson, and W. Greiner, J. Phys. G: Nucl. Part. Phys. **34**, 2073 (2007).
[32] S. K. Patra, F. H. Bhat, R. N. Panda, P. Arumugam, and R. K. Gupta, Phys. Rev. C **79**, 044303 (2009).
[33] H. Flocard, P. Quentin, and D. Vautherin, Phys. Lett. **B46**, 304 (1973).
[34] W. Koepf and P. Ring, Phys. Lett. **B212**, 397 (1988).
[35] J. Fink, V. Blum, P.-G. Reinhard, J. A. Maruhn, and W. Greiner, Phys. Lett. **B218**, 277 (1989).
[36] D. Hirata, H. Toki, I. Tanihata, and P. Ring, Phys. Lett. **B314**, 168 (1993).
[37] P. Möller, J. R. Nix, W. D. Wyers, and W. J. Swiatecki, At. Data Nucl. Data Tables **59**, 185 (1995); P. Möller, J. R. Nix, and K.-L. Kratz, *ibid.* **66**, 131 (1997).
[38] S. Yoshida, S. K. Patra, N. Takigawa, and C. R. Praharaj, Phys. Rev. C **50**, 1398 (1994); S. K. Patra, S. Yoshida, N. Takigawa, and C. R. Praharaj, *ibid.* **50**, 1924 (1994); S. K. Patra and C. R. Praharaj, *ibid.* **47**, 2978 (1993); J. P. Maharana, Y. K. Gambhir, J. A. Sheikh, and P. Ring, *ibid.* **46**, R1163 (1992).
[39] E. Chabanat, P. Bonche, P. Hansel, J. Meyer, and R. Schaeffer, Nucl. Phys. **A635**, 231 (1998).
[40] B. A. Brown, Phys. Rev. C **58**, 220 (1998).
[41] S. K. Patra and C. R. Praharaj, J. Phys. G: Nucl. Part. Phys. **23**, 939 (1997).
[42] Yu. Ts. Oganessian *et al.*, Phys. Rev. C **72**, 034611 (2005).
[43] G. Audi, A. H. Wapstra, and C. Thibault, Nucl. Phys. **A729**, 337 (2003).
[44] V. E. Viola, Jr. and G. T. Seaborg, J. Inorg. Nucl. Chem. **28**, 741 (1966).